proceedings

MDPI

Proceedings

Quality Analysis of a 3D-Printed Maraging Steel Part

César M. A. Vasques *, Pedro R. Resende, Adélio M. S. Cavadas and João C. C. Abrantes

proMetheus, Escola Superior de Tecnologia e Gestão, Instituto Politécnico de Viana do Castelo, Rua Escola Industrial e Comercial de Nun'Álvares, 4900-347, Viana do Castelo, Portugal

* Correspondence: cmavasques@gmail.com

Abstract: Like few other processes, additive manufacturing (AM) is reshaping the manufacturing industry's future; it can be used to manufacture, coat, or repair components with extremely high material requirements. In contrast to traditional, ablative manufacturing processes such as turning or milling, AM is a design-driven process that allows for significant design flexibility and fosters creativity. This article looks at 3D-printed metal objects made using the laser powder bed fusion technology. Uncertainties about the uniformity of powder raw material qualities and the mechanical properties of 3D printed maraging steel parts are examined. A demonstration maraging steel part is investigated as part of an ongoing research and discussed in terms of geometry and shape limitations, chemical composition, phases, microstructure and metallurgy, roughness, hardness, strength, and the effect of heat treatments, with the purpose of assessing the material homogeneity, its quality and the mechanical performance of 3D printed parts that can be used for the production and replacement of critical mechanical components using conventional manufacturing processes.

Keywords: Additive manufacturing; 3D printing; laser powder-bed fusion; maraging steel; 1.2709; mechanical properties; quality analysis.

Citation: Vasques, C. M. A.; Resende, P. R.; Cavadas, A.M.S.; Abrantes, J.C.C. Quality Analysis of a 3D-Printed Maraging Steel Part. *Proceedings* **2021**, *0*, 0. https://doi.org/

Received:
Accepted:
Published:

1. Introduction

Additive manufacturing (AM), like few other techniques, is transforming the manufacturing industry's future and can be used to build components with extremely high material requirements, regardless of shape, as well as prototypes and one-of-a-kind items in small and big quantities. In contrast to traditional, ablative manufacturing methods like as turning or milling, the design of AM determines the manufacturing process and this is why it is referred to as "design for additive manufacturing" (DfAM). While there are numerous additional AM laser methods, two have reached industrial maturity in the last 20 years: laser metal fusion and laser metal deposition. These technologies can be used to layer-by-layer manufacture complicated forms and individual metal components from metal powder in a rapid, flexible, sustainable and low-cost manner.

Research and development of AM and metal 3D-printing has during the last few years been growing very fast and directed to various aspects. Although metal AM techniques and terminology have been attempted to standardize [1], designations are diverse. The majority of these names are registered trademarks of various machine manufacturers. As a result, the description of these processes is prioritized by stressing their primary characteristics and highlighting their most important distinctions. This is to aid in the understanding of microstructure formation and the evolution of mechanical properties in components produced by the Laser Beam Melting (LBM), Electron Beam Melting (EBM), and Laser Metal Deposition (LMD) processes. A through discussion on the AM of metals was performed by Herzog et al. [2]. Recent review and relevant works regarding the 3D printing of maraging steels can also be found in [3–7].

This article looks at 3D-printed metal objects made using the Laser Powder Bed Fusion (LPBF) technology. Uncertainties about the uniformity of powder raw material qualities

and the mechanical properties of 3D printed maraging steel parts are examined. A demonstration maraging steel part is investigated as part of an ongoing research and discussed in terms of geometry and shape limitations, chemical composition, phases, microstructure and metallurgy, roughness, hardness, strength, and the effect of heat treatments, with the purpose of assessing the material homogeneity, its quality and the mechanical performance of 3D printed parts that can be used for the production and replacement of critical mechanical components using conventional manufacturing processes. Due to space limitations, only some selected aspects are detailed in this article. This field of research is relatively new, and this article aims to contribute to a still fragmented body of knowledge regarding the production of 3D printed maraging steel parts through the lens of a systematized approach to evaluating the quality of AM products.

2. Materials and Methods

Known by many names, powder bed melting (or fusion), as an AM process in which thermal energy selectively fuses regions of a powder bed, is currently the most common type of metal 3D printing. These machines distribute a fine layer of powder over a build plate and selectively melt a cross section of the part into the powder layer. There are two distinct types of powder bed melting techniques: Selective Laser Melting (SLM) and Electron Beam Melting (EBM); the former is more of concern here in this study. SLM is also known interchangeably as Direct Metal Laser Sintering (DMLS), Selective Laser Sintering (SLS), Direct Metal Printing (DMP) or Laser Powder Bed Fusion (LPBF). The majority of powder bed fusion machines are SLM machines which fuse metal layers together using high-powered lasers. Following a print, an operator removes the parts from the powder bed, cuts them free from the build plate, and post processes them. It is the current industry standard for metal printing and the majority of companies now sell SLM machines.

Steel is a widely used engineering material, and many of the alloys that are easily welded and cast are excellent candidates for AM processes. Carbon steels, alloy steels, stainless steels, and tool steels are the four major categories of steel alloys. Maraging steels are high-alloy steels that contain between 15% and 25% Ni as the primary alloying element and have a low carbon content. They are based on the formation of a soft martensite that is strengthened by the formation of intermetallic compounds during the aging process. While maraging steels are not technically tool steels, due to their superior strength, malleability, and thermal stability, they can be used for that purpose and are therefore referred to sometimes as "tool steels". Alternative commercial/standardized names/designations for similar feedstock steel powder material to that used in this work have been employed, e.g., M300 Tool Steel (LPW), 1.2709 (EN 10027-2; SLM Solutions; SANDVIK), Maraging Steel (3D Systems), CL 50WS (Concept Laser), MS1 (EOS), Tool Steel 1.2709-A LMF (TRUMPF), X3NiCoMoTi 18-9-5 (DIN EN 10027-1) and 18Ni-300 (MIL-S-46850D).

Specifically, the maraging steel 1.2709 is a pre-alloyed ultra high strength steel in the powder form. Its composition corresponds to US classification 18% Ni Maraging 300, European 1.2709 and German X3NiCoMoTi 18-9-5. Maraging steels have a high strength-to-toughness ratio without sacrificing ductility, weldability, or dimensional stability as they age. The majority of maraging steel grades have martensite start formation temperatures in the range of 200 to 300 degrees Celsius and are fully martensitic at room temperature. As a result, retained austenite is generally not a problem in these alloys, and refrigeration treatments prior to aging are not required. Typically, the martensite is a low-carbon, body-centered cubic (BCC) lath martensite with a high dislocation density but no twinning. As built and untreated the 1.2709 has yield and tensile strength in the order of 1000$\pm$100 MPa and 1100$\pm$100 MPa, 8$\pm$3% elongation and hardness 33-37 HRC; in the aged hardened state these values become 1900$\pm$100 MPa, 1950$\pm$100 MPa, 2$\pm$1% and 50-54 HRC, respectively (cf. [8]). These characteristics make maraging steel an attractive material for use with AM in the automotive industry for drive shafts, gears, springs, and heavy-duty transmissions; in the aerospace industry for rocket and missile skins; in the sports industry for fencing

Table 1. Typical chemical composition of the Tool Steel 1.2709-A LMF (TRUMPF) powder (wt%) and SEM measured values [7,8].

	Ni	Co	Mo	Ti	Cr	Al	Si,Mn	S,P	C	Fe
Nominal	17-19	8.5-11	4.5-6	0.6-1.2	<0.5	0.05-0.15	<0.1	<0.01	<0.03	balance
Measured	14.39	10.73	4	1.36	–	–	–	–	–	balance

blades, bicycle frames, and golf club heads; and in various industries for machinery and tooling.

The 3D-printed part that was studied in this research is shown in Figure 1, which is a demonstration part made of maraging steel feedstock powder with reference Tool Steel 1.2709-A LMF provided by TRUMPF and that was 3D printed on our Truprint 1000 machine facilities with a printing time of around 6 hours. As can be seen, In figure 1 (top images) the part was printed in middle cylinder and the final part is connected (fused) into the steel substrate plate. A precision cutting machine Struers Accutom-2 with a diamond cut-off wheel was used to cut the part from the substrate plate and to cut a material sample (red line in the bottom image) for closer material quality analysis and inspection.

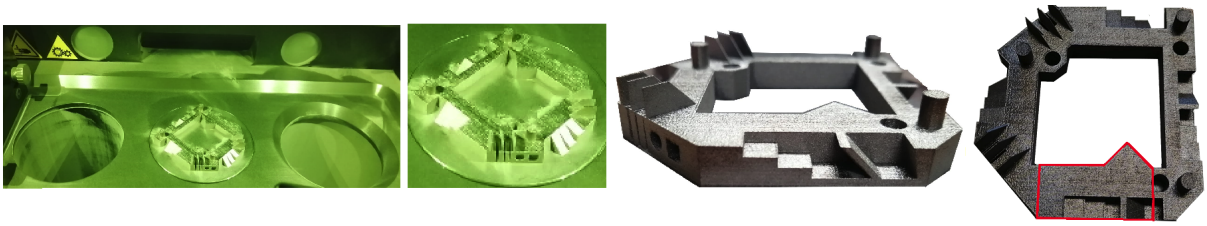

Figure 1. 3D-printed studied part as built on the substrate plate inside in the machine (left); final part and cut material sample (right).

3. Results and Discussion

The feedstock powder used to produce the demonstration part with reference Tool Steel 1.2709-A LMF was provided by TRUMPF. Particle size distribution, morphology and chemical composition analyses were performed to verify the quality of the powder. The morphology and chemical composition of the same sample of powder were determined using a Scanning Electron Microscope (SEM) model Hitachi SU1510EM, and the particle size distribution was determined using a laser diffraction particle size analyzer, model Malvern MS3000, for fast, accurate and reliable analysis. The particle morphology can be visualized in Figure 2 and, in general, the particles present a spherical shape, with low particles agglomeration and irregularities on the particle surface, indicating a high quality powder with a low possibility of defects. A detailed image of a spherical particle surface at 3000× is also shown in Figure 3. The chemical composition analysis was obtained by SEM coupled with a Bruker Quantax 200 detector for Energy-Dispersive X-ray Spectroscopy (EDS) analysis, and showed small differences when compared with the typical material suppliers, as can be seen in Table 1.

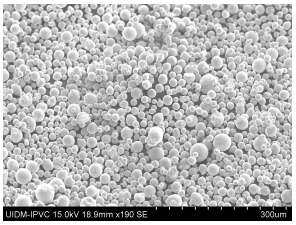

Figure 2. SEM images at 190× magnification of Tool Steel 1.2709-A LMF (TRUMPF) powder particle.

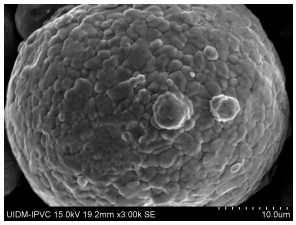

Figure 3. SEM images at 3000× magnification of Tool Steel 1.2709-A LMF (TRUMPF) powder particle.

As expected, the particle size distribution in Figure 4 follows a typical Gaussian-like distribution, with d_{10}= 17.5 , d_{50}= 29.8 and d_{90}= 50.7 μm. However, the values are slightly

lower compared to commercial suppliers whose size range is between 20 to 60 μm [9]. Furthermore, in Figure 2, it is possible to observe a substantially high amount of satellite particles with reduced diameter, about 15 μm. It's worth noting that powder particles smaller than 10 or 20 μm are detrimental to the flowability of the powder and should be avoided, but no issues were detected during the manufacturing. The powder was spread evenly and smoothly across a bed and formed a uniform layer with no air voids, a consequence of the good surface quality and uniform particle morphology of the powder sample, necessary for good flowability [10]. For this reason, no significant defects were detected in the surface of the built-part, like porosities, and it was possible to obtained lower roughness. Numerous tests were run to reduce the relative standard deviation, as illustrated in Figure 4, where 5 analyses were run for each of the 8 tests shown.

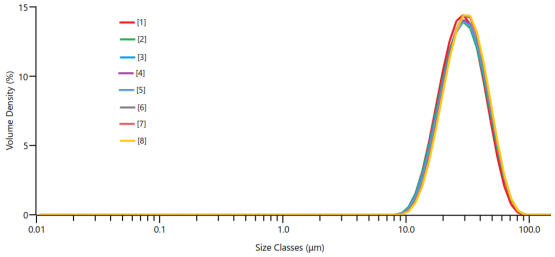

Figure 4. Particle size distribution of Tool Steel 1.2709-A LMF (TRUMPF) powder; five analyses were run for each of the eight tests shown.

The demonstration maraging steel 3D-printed part depicted in Figure 1 was printed in approximately 6 hours, without the need for any supports, directly from the WZA file provided by the TRUMP Build Processor, and in the lay down position shown. It demonstrates an excellent visual aspect, dimensional quality, and repeatability, even for more complex details such as thin shark fins, inclined planes and extrusions, and cylindrical and square-shaped holes.

This section discusses also the results of a two-dimensional surface roughness measurement with Ra as the measured quantity. Two roughness measurement devices were used, namely, the rugosimeter Mituttoyo Sj-210 and with the SEM, and two types of surfaces were investigated. 3D printing technology has enabled that metallic parts fabricated with the SLM method have mechanical properties that are higher in comparison with traditionally produced ones [11,12]. Nevertheless, an obvious drawback of 3D printed parts, in general, and SLM parts, in particular, is the large surface roughness caused by the nature of the fabricating process as investigated in [13–16]. There are many different roughness parameters in use, but Ra, the arithmetic average value of filtered roughness profile determined from deviations about the center line within an evaluation length, is by far the most common, though this is often for historical reasons and not for particular merit, as the early roughness meters could only measure Ra. The arithmetical mean deviation of the assessed profile along a line on 3D-printed SLM parts could range from 5 to 50 μm, and is primarily found below 20 μm as in [14].

The results of a two-dimensional surface roughness measurement with Ra as the measured quantity were obtained as follows. We began by measuring the 2D surface roughness of the exterior surface along the represented measurement line using the Mituttoyo Sj-210, as illustrated in Figure 5. We calculated the average of the surface roughness values, Ra; the value obtained for the exterior part is Ra = 5.39 μm, where all the surface roughness results from all measures were averaged. As can be seen, the Ra values are within the standard aforementioned range, i.e., less than 20 μm. Additionally, we used an Hitachi SU1510 SEM to determine the respective roughness. We obtained a value for Ra = 5.75 μm using this method, and in Figure 6 a 3D image of the measure is shown. As a result, we can conclude that the obtained average Ra values are within the expected range for SLM parts and that good surface quality was achieved in terms of roughness since the obtained values fall within the initial value of the typical and expected range.

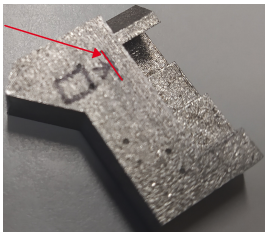

Figure 5. Material sample and roughness measurement line.

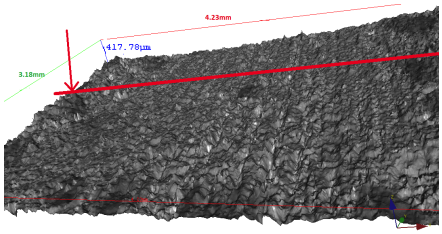

Figure 6. Roughness surface measured with the SEM.

The density of the maraging steel we measured according to the buoyancy method – Archimedes principle, in distilled water. Archimedes principle states that a body immersed partially or fully in fluid experiences a buoyant force acting upwards on it. The magnitude of this force is equivalent to the weight of the fluid displaced by the body. The solid is weighed in air and then again in the auxiliary liquid with a known density. The density of the maraging steel $\rho = \rho_{H_2O}/[1 - (m_a/m)]$ can therefore be calculated from the measured values of true and apparent (immersed) masses, m and m_a, respectively. The density obtained with this method for the 3D printed maraging steel is 7,909 kg/m^3 which compares very well with the reference value of 8,100 kg/m^3 for the non-printed material [17]; in the experimental procedure a weighing system with 1 centigram was used where the true and apparent measured masses were $m = 121.41$ and $m_a = 106.06$ grams.

A qualitative experimental phase analysis was performed by X-ray powder diffraction (XRD) using a conventional Bragg–Brentano diffractometer (Bruker D8 Advance DaVinci, Karlsruhe, Germany) with Ni-filtered Cu-Kα radiation (λ = 1.5406 Å) produced at 40 kV and 40 mA, with a linear detector (Lynxeye 1-D). Data sets were recorded in the 2θ range of 20 to 120° with a step size of 0.02°, with 0.5 s per step size, and with a spin rate of 15 rpm. The Rietveld refinements were performed using the software TOPAS 5.0 (Bruker AXS, Karlsruhe, Germany) with the fundamental parameters approach. As can be seen on Figure 7, XRD measurements taken on the 3D-printed sample show a single-phase material with a body-centered cubic (BCC) structure (space group Im-3m). Site occupancy parameters used in Rietveld refinements are in agreement with the elementary nominal composition obtained from the feedstock powder manufacturers (Table 1), with Mo, Co, Ni and Ti in solid solution in the iron crystal lattice. The lattice parameter obtained was 0.28799661 nm, with a subsequent theoretical density of 8,216 kg/m^3, and with a crystallite size of 26 nm, probably too low due to the rapid cooling rate during the material fusion of the AM 3D-printing process.

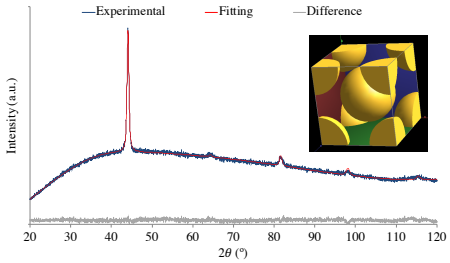

Figure 7. XRD pattern of 3D printed material sample.

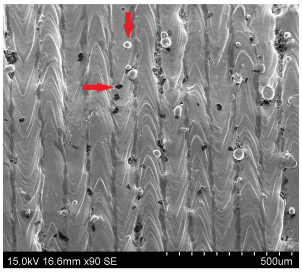

Figure 8. SEM image of the surface built part at 90x magn.

The external top surface of the part analyzed, where the roughness was measured, can be visualized in Figure 8. The image was acquired using a SEM, and it reveals welding lines with a width of approximately 100 μm and a high degree of material agglomeration, as indicated by the arrows, which was possibly caused by the combination of the high laser intensity and the small diameter of the satellite particles. The chemical composition of the built part on the surface showed to be different from the powder particles, as can be observed in Table 2. The significant difference is the increase in Ti and decrease in Fe and Ni, meaning that there was an accumulation of Ti, creating Ni-Fe-Ti intermetallic

compounds (IC), identified by the black agglomerations in Figure 8. However, the chemical composition of the built part on the surface without Fe-Ni-Ti particles, is similar to the powder composition, as shown in Table 2.

Table 2. Comparison of the measured chemical composition (wt%) between maraging steel powder and built part of Tool Steel 1.2709-A LMF (TRUMPF); surface average with and without the extraneous concentrations of Ni-Fe-Ti intermetallic compounds (IC).

	Ni	Co	Mo	Ti	Fe
Powder	14.39	10.73	4.00	1.36	61.61
Part surface (with IC)	12.81	7.40	3.28	8.87	48.31
Part surface (without IC)	14.64	7.60	3.21	1.13	60.28

The Rockwell hardness scale is a measurement of a material's indentation hardness. In this work, we analyzed the Rockwell hardness of a cut sample of the 3D-printed tool steel part on both the top and lateral surfaces using a hardness tester machine with an electronically controlled test cycle, model EmcoTest DuraVision 20G5. To make a preliminary assessment, five different hardness measurements were taken at random locations, yielding a reasonably close range of values with low dispersion, namely 30.15, 34.95, 34.08, 34.82, and 34.25 HRC, with an expected value of 33.65 $\pm$1.561HRC ($\pm$4.64%) for a confidence level of 95%, precluding the need for further measurements. Tensile strength and hardness are both measures of a metal's resistance to deformation due to plastic deformation. As a result, they are roughly proportional. When metals are tested, indentation hardness is linearly related to tensile strength and can be used to estimate the tensile properties of the material in a non-destructive manner [18]. A straightforward conversion of HRC to Brinell hardness (HB) using recommendation formulas [19] gives $8.570 \times \text{HRC} + 27.6 = 316$ HB and the tensile strength R_m = 1,050 MPa. As a rule of thumb, for most steels, the HB and the tensile strength my be related by multiplying the Brinell hardness by 3.45 yielding as another estimate of the ultimate tensile strength R_m = 1,090 MPa. Lastly, using the equations for converted hardness value to Vickers in [18], yielding 333 HV, we get the following nominal values of the yield stress as $R_{p0.2} = -90.7 + 2.876 \times 333 = 867$ MPa and the tensile strength $R_m = -99.8 + 3.734 \times 333 = 1{,}144$ MPa. While these values differ slightly since they are obtained by different methods based on empirical rules they are in the expected order of magnitude. As such, both values of hardness and tensile ultimate strength are well in line with those reported by the manufacturer and in the open literature, namely $R_{p0.2}$ = 1,000 $\pm$100 MPa and R_m = 1,100 $\pm$100 MPa, demonstrating that the hardness test can in a straightforward and non-destructive way be used to estimate the maraging steel strength.

4. Conclusion

This article examines 3D-printed metal objects created via laser powder bed fusion (LPBF) technology and the uncertainties surrounding the uniformity of powder raw material qualities and the mechanical properties of 3D printed maraging steel parts. Due to space constraints, this article will discuss only a few selected aspects of an ongoing research project. Visual inspection of the demonstration 3D-printed part revealed the part's exceptional dimensional quality, despite the fact that it contains some geometrically complex details. The material composition of the feedstock powder was found to differ slightly from the nominal Ni values but had no discernible effect on mechanical performance. The metallurgical properties of maraging steels were discussed and the most significant ones were identified experimentally. Theoretical calculations of the density of the material using XRD and SEM agree very well with the experimental results, indicating that the material has very little porosity and defects. The obtained surface roughness of the part was also excellent and within the best indicated values for similar equipments in use. The overall quality of the 3D-printed part is excellent, and the predictability of its strength based on simplified non-destructive hardness measurements demonstrates a successful application of additive manufacturing (AM) and laser powder LPBF technology to create

critical mechanical components with increased mechanical performance and reduced mass to strength ratios through the use of maraging steels. This field of research is still in its youth, and this article contributes to a still fragmented body of knowledge regarding the production of 3D printed maraging steel parts and the use of a systematic approach to evaluating their quality, enabling AM to be used for the production and replacement of critical mechanical components manufactured with conventional processes.

Acknowledgments: The authors gratefully acknowledge the support provided by the Foundation for Science and Technology (FCT) of Portugal, within the scope of the project of the Research Unit on Materials, Energy and Environment for Sustainability (proMetheus), Ref. UID/05975/2020, financed by national funds through the FCT/MCTES.

References

1. ASTM. Terminology for Additive Manufacturing Technologies (ASTM F2792-12a), 2012. doi:10.1520/f2792-12a.
2. Herzog, D.; Seyda, V.; Wycisk, E.; Emmelmann, C. Additive manufacturing of metals. *Acta Materialia* **2016**, *117*, 371–392. doi:10.1016/j.actamat.2016.07.019.
3. Takata, N.; Nishida, R.; Suzuki, A.; Kobashi, M.; Kato, M. Crystallographic features of microstructure in maraging steel fabricated by selective laser melting. *Metals* **2018**, *8*, 440. doi:10.3390/met8060440.
4. Song, J.; Tang, Q.; Feng, Q.; Ma, S.; Setchi, R.; Liu, Y.; Han, Q.; Fan, X.; Zhang, M. Effect of heat treatment on microstructure and mechanical behaviours of 18Ni-300 maraging steel manufactured by selective laser melting. *Optics & Laser Technology* **2019**, *120*, 105725. doi:10.1016/j.optlastec.2019.105725.
5. Wu, W.; Wang, X.; Wang, Q.; Liu, J.; Zhang, Y.; Hua, T.; Jiang, P. Microstructure and mechanical properties of maraging 18Ni-300 steel obtained by powder bed based selective laser melting process. *Rapid Prototyping Journal* **2020**, *26*, 1379–1387. doi:10.1108/rpj-08-2018-0189.
6. Yao, Y.; Wang, K.; Wang, X.; Li, L.; Cai, W.; Kelly, S.; Esparragoza, N.; Rosser, M.; Yan, F. Microstructural heterogeneity and mechanical anisotropy of 18Ni-330 maraging steel fabricated by selective laser melting: The effect of build orientation and height. *Journal of Materials Research* **2020**, *35*, 2065–2076. doi:10.1557/jmr.2020.126.
7. Mooney, B.; Kourousis, K. A review of factors affecting the mechanical properties of maraging steel 300 fabricated via laser powder bed fusion. *Metals* **2020**, *10*, 1273. doi:10.3390/met10091273.
8. Maraging Steel 1.2709 - Protolabs. www.protolabs.co.uk/media/1022869/maraging-steel-1.pdf. Accessed: 16-September-2021.
9. Pannitz, O.; Sehrt, J.T. Transferability of Process Parameters in Laser Powder Bed Fusion Processes for an Energy and Cost Efficient Manufacturing. *Sustainability* **2020**, *12*.
10. Yun, H.; Dong, L.; Wang, W.; Bing, Z.; Xiangyun, L. Study on the flowability of TC4 Alloy Powder for 3D Printing. *IOP Conference Series: Materials Science and Engineering* **2018**, *439*, 042006. doi:10.1088/1757-899x/439/4/042006.
11. Pagáč, M.; Hajnyš, J.; Petrů, J.; Zlámal, T. Comparison of Hardness of Surface 316L Stainless Steel Made by Additive Technology and Cold Rolling. *Materials Science Forum* **2018**, *919*, 84–91. doi:https://doi.org/10.4028/www.scientific.net/msf.919.84.
12. Liverani, E.; Toschi, S.; Ceschini, L.; Fortunato, A. Effect of selective laser melting (SLM) process parameters on microstructure and mechanical properties of 316L austenitic stainless steel. *Journal of Materials Processing Technology* **2017**, *249*, 255–263. doi:https://doi.org/10.1016/j.jmatprotec.2017.05.042.
13. Strano, G.; Hao, L.; Everson, R.M.; Evans, K.E. Surface roughness analysis, modelling and prediction in selective laser melting. *Journal of Materials Processing Technology* **2013**, *213*, 589–597. doi:https://doi.org/10.1016/j.jmatprotec.2012.11.011.
14. Wang, D.; Liu, Y.; Yang, Y.; Xiao, D. Theoretical and experimental study on surface roughness of 316L stainless steel metal parts obtained through selective laser melting. *Rapid Prototyping Journal* **2016**, *22*, 706–716. doi:https://doi.org/10.1108/RPJ-06-2015-0078.
15. Leary, M. 4 - Surface roughness optimisation for selective laser melting (SLM): Accommodating relevant and irrelevant surfaces. In *Laser Additive Manufacturing*; Brandt, M., Ed.; Woodhead Publishing Series in Electronic and Optical Materials, Woodhead Publishing, 2017; pp. 99–118. doi:https://doi.org/10.1016/B978-0-08-100433-3.00004-X.
16. Vayssette, B.; Saintier, N.; Brugger, C.; Elmay, M.; Pessard, E. Surface roughness of Ti-6Al-4V parts obtained by SLM and EBM: Effect on the High Cycle Fatigue life. *Procedia Engineering* **2018**, *213*, 89–97. 7th International Conference on Fatigue Design, Fatigue Design 2017, 29-30 November 2017, Senlis, France, doi:https://doi.org/10.1016/j.proeng.2018.02.010.
17. Wikipedia. Maraging steel — Wikipedia, The Free Encyclopedia. http://en.wikipedia.org/w/index.php?title=Maraging%20steel&oldid=1031815960, 2021. [Online; accessed 16-September-2021].
18. Pavlina, E.; Tyne, C.V. Correlation of yield strength and tensile strength with hardness for steels. *Journal of Materials Engineering and Performance* **2008**, *17*, 888–893. doi:10.1007/s11665-008-9225-5.
19. Iron-Foundry. Rockwell Hardness (HRC, HRB) to Brinell Hardness (HB or BHN) Conversion. http://www.iron-foundry.com/hardness-hrc-hrb-hb.html, 2021. [Online; accessed 13-September-2021].